Two-Way Cognitive Network supported by Reconfigurable Intelligent Surface

1st Thu-Thuy Thi Dao
Faculty of Electrical and Electronics Engineering
Ho Chi Minh City University of Technology and Education
Ho Chi Minh City, Vietnam
thuydtt.ncs@hcmute.edu.vn
Faculty of Electronics Technology
Industrial University of Ho Chi Minh City
Ho Chi Minh City, Vietnam
daothithuthuy@iuh.edu.vn

2nd Pham Ngoc Son
Faculty of Electrical and Electronics Engineering
Ho Chi Minh City University of Technology and Education
Ho Chi Minh City, Vietnam
sonpndtvt@hcmute.edu.vn

***Abstract*—In this paper, we propose an underlay two-way scheme in which two secondary sources transmit simultaneously their data to each other through the Reconfigurable Intelligent Surface (RIS). The proposed scheme is designed to operate in the full-duplex mode under an interference constraint of a primary receiver (PR), called the RIS-UTW scheme. The exact closed-form expressions of outage probabilities are considered to evaluate the system performance. The results show that the secondary system performance increases as the number of reflected elements, the distances between PR and secondary sources, the maximum interference power-to-plus-noise ratio at primary receivers, and the maximum signal-to-plus-noise ratio at the secondary sources increase. Moreover, if the value of the maximum interference power-to-plus-noise ratio at primary receivers or the maximum signal-to-plus-noise ratio at the secondary sources is large enough, the outage probabilities of the secondary network will fall into a saturation state. Finally, the Monte Carlo simulation results are collected to evidence the validity of the analytical expressions of the outage probabilities.**

***Index Terms*—Underlay two-way scheme, reconfigurable intelligent surface, full-duplex.**

I. Introduction

Nowadays, the growing number of users and increasingly diverse mobile multimedia applications lead to a rising challenge about using frequency spectral efficiency (SE), energy efficiency (EE), and cost-efficiency in the deployment and operation of wireless networks. Recently, Reconfigurable Intelligent Surface has been considered as an emerging cost-saving technology for future wireless communication systems. These artificial surfaces include reconfigurable electromagnetic materials that can be controlled and programmed using integrated electronics and integrated into the existing infrastructure [1]. In particular, RIS is able to change the signal transmission direction with low-cost passive devices. In this way, RIS is able to create favorable wireless propagation environments without consuming power. Furthermore, RIS can be readily coated on the facades of buildings, which reduces implementation cost and complexity. In addition, RIS passively reflects the signal without processing while a relay actively processes the received signal before re-transmitting. Lead to the RIS-assisted communication outperforms the conventional relaying techniques in terms of spectrum and energy efficiency [2], [3].

Besides, two-way relay cooperation networks are also one of the solutions to enhance the system performance and SE because of their ability to exchange signals of two device users over the same shared channel, especially in full-duplex communication [4]–[6].

In addition, the authors in [7] shown that the utilization of the licensed frequency spectrum versus time and space is low. Thus the cognitive radio (CR) network was proposed to allow the primary network to share its frequency band with the secondary network to improve SE. In CR networks, there are three protocols (underlay, overlay, and interweave) were proposed so the secondary users can operate flexibly and smartly to access the licensed frequency spectra of the primary users as long as the primary network still maintains the quality of services [8]–[10]. The cognitive two-way relay networks combined with other techniques are considered and valuated under an interference constraint of a primary receiver [11]–[13].

A. Related work and motivation

In [3], the authors analyzed and compared the performance of two wireless systems with aid of RIS and amplify-and-forward (AF) relaying. The results showed that RIS-assisted wireless systems outperform the corresponding AF-relaying ones. To take advantage of both SE and EE, the one-way cognitive network had multiple primary receivers (PR) and a single secondary receiver (SR) combined with a RIS half-duplex [14] and full-duplex [15] or multiple RISs [16].

Recently, the two–way communications via RIS where two users communicate through a common RIS were investigated [17], [18]. In [17], outage probability and average throughput were derived with assuming that uplink and downlink communication channels between two users and the RIS can be reciprocal. In [18], the channels between the two users and RIS can either be reciprocal or non-reciprocal, and the authors proposed the optimal phases and approximation methods for

each case to derive the outage probability and the SE of the system.

Motivated by previous works for a two-way network to improve SE and EE, we suggest a RIS-supported underlay two-way scheme, called as RIS-UTW, in which two secondary sources operate in the full-duplex mode with aid of a RIS under the limit condition of a primary receiver.

To consider and evaluate the system performance, the outage probability of the system is investigated according to parameters such as the maximum interference power - to -plus-noise ratio that the PR can decode information in the primary network (Q); the maximum signal-to-plus-noise ratio that the secondary network hardware can satisfy (SNR); the relative position of the RIS and the PR; the change in the number of reflected elements of the RIS; and the loop interference suppression ability of the full-duplex transmission.

B. Contributions

The contributions in this paper are summarized as follows. Firstly, the exact and asymptotic expressions of the outage probabilities of two sources in the proposed scheme are analyzed, verified, and proved valid by the simulation results. The paper examines the parameters affecting the outage probabilities of the secondary system. Secondly, the simulation and analysis results show that the number of reflected elements or the distance between PR and secondary sources increase, the outage probabilities of the two secondary sources decrease. Addition on, with any number of reflected elements, the outage probabilities of both sources decrease quickly when Q increases in a small value region, and attains a saturation value in the greater Q region. Finally, the lines OP of the sources versus $Pmax/N_0$ (dB) also decreases when $Pmax/N_0$ (dB) is less than about -10(dB), then the OP stays at the same value even though $Pmax/N_0$ (dB) still increases.

C. Paper organization and notations

This paper is organized into sections as follows. Section 2 presents the proposed system model. Section 3 analyzes outage probabilities. Results and discussions are shown in section 4. Lastly, section 5 is the conclusion.

The notations: $f_\Lambda(\cdot)$ and $F_\Lambda(\cdot)$ present respectively the probability density function (PDF) and the cumulative distribution function (CDF) of a random variable (RV) Λ; $\Pr[\Xi]$ presents the probability operation of an event Ξ; $\Gamma[.]$ is the Gamma function [19] (eq.8.310); $\gamma[.,.]$ is the lower incomplete Gamma function [19] (eq.8.350.1); $\Gamma[.,.]$ is the upper incomplete Gamma function [19] (eq.8.350.2); $W,()$ is the Whittaker function [19] (eq.9.222); $CN()$ denotes the complex normal distribution.

II. System model

A system model of RIS-supported underlay two-way network is shown in Figure 1 in which two-antenna secondary sources S_1 and S_2 send simultaneously their data x_1 and x_2 ($x_1 \in \mathrm{S}_1$ and $x_2 \in \mathrm{S}_2$) to each other through an RIS with T metasurfaces MS_t , $t = \{1, 2, ..., T\}$. The S_1 and S_2 the

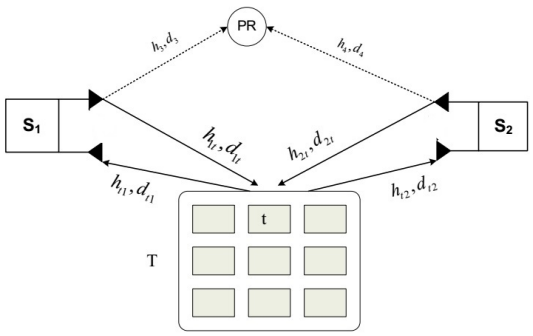

Fig. 1. System model of an RIS-supported underlay two-way network

tolerate interference constraint of the primary receiver, denoted as I. In Figure 1,(h_{1t}, d_{1t}), (h_{t1}, d_{t1}), (h_{2t}, d_{2t}), (h_{t2}, d_{t2}), (h_3, d_3) and (h_4, d_4) denote the fading channel coefficients and the normalized distances of links $S_1 - MS_t, MS_t - S_1, S_2 - MS_t, MS_t - S_2, S_1 - PR$ and $S_2 - PR$, respectively. We have some assumptions as: 1) direct links between node pairs (S_1, S_2) and (MS_t, PR) does not exist due to the far distance, deep shadow fading or beamforming of the RIS; 2) additive noises at the S_1 and S_2 are $CN(0, N_0)$ with zero-mean and identical variance N_o; 3) each MS_t is close to others, and thus the normalized distances can be set as $d_{1\mathrm{t}} = d_{\mathrm{t}1} = d_1$, $d_{2\mathrm{t}} = d_{\mathrm{t}2} = d_2$; 4) wireless channels between node pairs (S_1, MS_t) and (S_2, MS_t) are reciprocal, i.e $h_{t1} = h_{1t}$ and $h_{t1} = h_{1t}$ [18]; all fading channel coefficients are complex normal RVs, i.e. $h_{t1} = h_{1t} = |h_{1t}|\, e^{\varphi_{1t}} \in CN(0, 1/\lambda_1)$, $h_{t2} = h_{2t} = |h_{2t}|\, e^{\varphi_{2t}} \in CN(0, 1/\lambda_2)$, $h_3 \in CN(0, 1/\lambda_3)$ and $h_4 \in CN(0, 1/\lambda_4)$, where φ_{1t} and φ_{2t} are phase values of reciprocal channels h_{1t} and h_{2t}, $\lambda_{\mathrm{u}} = d_{\mathrm{u}}^{\beta}$, β is a path-loss exponent, and $u \in \{1, 2, 3, 4\}$; 5) Loop-back signals from the transmit antenna to the receive antenna are filtered to cancel completely.

Under operation conditions of the underlay cognitive radio network, the transmit power of the secondary sources S_q (denoted by P_q, $\mathrm{q} \in \{1, 2\}$) must be below a maximum power (denoted by $P_{\mathrm{q,max}}$) and satisfies the interference constraint of the primary network. Therefore, P_q is set maximally as [20]

$$P_{\mathrm{q}} = \min\left(P_{\mathrm{q,max}}, I/g_{(q+2)}\right) \tag{1}$$

where $g_{(q+2)} = \left|h_{(q+2)}\right|^2$.

At the same time, the secondary sources S_1 and S_2 send simultaneously the data x_1 and x_2 respectively to each other through the RIS with the same frequency. More specifically, the S_1 will receive the signal including the desired data x_2, and is affected by self-interference signal including the own data x_1 from the reverse reflection of the RIS, and by internal additive noise. The received signal at the S_1 is presented as

[17], [18].

$$y_1 = \underbrace{\sqrt{P_2}x_2\left(\sum_{t=1}^{T} h_{2t}r_t h_{t1}\right)}_{\text{Desired signal}} + \underbrace{\sqrt{P_1}x_1\left(\sum_{t=1}^{T} h_{1t}r_t h_{t1}\right)}_{\text{Self-inteference signal}} + n_1 \tag{2}$$

where r_t is the unit-adjusted response of the MS_t and can be expressed as $r_t = e^{j\phi_t}$, ϕ_t is the adjustable phase induced by the MS_t; the additive Gaussian noise n_1 is $CN(0, N_0)$ and $\mathrm{E}\left\{|x_1|^2\right\} = \mathrm{E}\left\{|x_2|^2\right\} = 1$.

In (2), the S_1 can cancel perfectly the self-inference signal $\sqrt{P_1}x_1\left(\sum_{t=1}^{T} h_{1t}r_t h_{t1}\right)$ because of holding the parameters h_{1t}, h_{t1} and r_t in the setup phase and combining with own parameters P_1 and x_1. In addition, the phase ϕ_t of the MS_t is selected optimally as $\phi_t = -(\varphi_{1t} + \varphi_{2t})$ [3], [17], [18]. The formula (2) is rewritten as

$$y_1 = \sqrt{P_2}x_2\left(\sum_{t=1}^{T} |h_{t1}| \times |h_{2t}|\right) + n_1 \tag{3}$$

Hence, the received signal-to-interference-plus-noise ratio (SINR) at the S_1 to decode x_2 is obtained from (3) as

$$\gamma_1 = \frac{\left|\sqrt{P_2}x_2\left(\sum_{t=1}^{T} |h_{t1}| \times |h_{2t}|\right)\right|^2}{|n_1|^2} = \frac{P_2\left(\sum_{t=1}^{T} |h_{t1}| \times |h_{2t}|\right)^2}{N_0}, \tag{4}$$

For simplicity in analyses, we set as $P_{1,\max} = P_{2,\max} = P_{\max}$. In addition, we also defined as

$$\gamma_0 = P_{\max}/N_0, Q = I/N_0, \Psi = \sum_{t=1}^{T} |h_{t1}| \times |h_{2t}|. \tag{5}$$

Substituting in (1) and (5) into (4), we have:

$$\gamma_1 = \min(\gamma_0, \frac{Q}{g_4})\Psi^2, \tag{6}$$

Similarly, the received signal and the SINR at the S_2 to decode x_1 are inferred respectively as

$$y_2 = \underbrace{\sqrt{P_1}x_1\left(\sum_{t=1}^{T} h_{1t}r_t h_{t2}\right)}_{\text{Desired signal}} + \underbrace{\sqrt{P_2}x_2\left(\sum_{t=1}^{T} h_{2t}r_t h_{t2}\right)}_{\text{Self-inteference signal}} + n_2, \tag{7}$$

$$\gamma_2 = \frac{P_1\left(\sum_{t=1}^{T} |h_{1t}| \times |h_{t2}|\right)^2}{N_0} = \min(\gamma_0, \frac{Q}{g_3})\Psi^2, \tag{8}$$

where the additive Gaussian noise n_2 is $CN(0, N_0)$.

III. Outage probability analysis

The outage probability of the secondary source S_p occurs when the S_p cannot successfully decode the desired data x_w of the opposite secondary source S_w in one transmission phase, $(p, w = \{1, 2\})$ and $p \neq w$. This probability is defined as $OP_{S_p}^{out} = \Pr\left[R_{S_p} < R_{th}\right]$, where R_{S_p} is the achievable data rate at the S_p and is expressed as $R_{\mathrm{S_p}} = \log_2(1 + \gamma_{\mathrm{p}})$, and R_{th} is the threshold data rate (bits/s/Hz). The outage probability of the S_p in RIS-UTW scheme is presented as

$$\begin{aligned} OP_{S_p}^{out} &= \Pr\left[\gamma_p < 2^{R_{th}} - 1\right] \\ &= \Pr\left[\min(\gamma_0, \tfrac{Q}{g_{(\mathrm{w}+2)}})\Psi^2 < \underbrace{\left(2^{R_{th}} - 1\right)}_{\alpha_1}\right] \\ &= \underbrace{\Pr\left[\gamma_0\Psi^2 < \alpha_1, \gamma_0 < \frac{Q}{g_{(\mathrm{w}+2)}}\right]}_{\Upsilon_1} + \\ &\quad + \underbrace{\Pr\left[\frac{Q}{g_{(\mathrm{w}+2)}}\Psi^2 < \alpha_1, \gamma_0 \geq \frac{Q}{g_{(\mathrm{w}+2)}}\right]}_{\Upsilon_2} \end{aligned} \tag{9}$$

To analyze the probability $OP_{S_p}^{out}$ in (9), the CDF and PDF of the RV Ψ are presented by Lemma 1.

Lemma 1: From (5), Ψ is the sum of T independent and identical double Rayleigh RVs, the PDF of the Ψ can be tightly approximated as the first term of a Laguerre series expansion [21] (eq.2.76). The PDF and CDF of the RV Ψ is obtained respectively as [3]

$$f_\Psi(x) \simeq \frac{x^a}{b^{a+1}\Gamma(a+1)}\exp\left(-\frac{x}{b}\right) \tag{10}$$

$$F_\Psi(x) \simeq \frac{\gamma\left(a+1, \frac{x}{b}\right)}{\Gamma(a+1)} \tag{11}$$

where $a = \frac{k_1^2}{k_2} - 1$, $b = \frac{k_2}{k_1}$, $k_1 = \frac{T\pi}{4\sqrt{\lambda_1\lambda_2}}$, and $k_2 = \frac{T}{\lambda_1\lambda_2}\left(1 - \frac{\pi^2}{16}\right)$.

The Υ_1 in the (9) is determined as followed

$$\begin{aligned} \Upsilon_1 &= \Pr\left[\Psi < \sqrt{\tfrac{\alpha_1}{\gamma_0}}, g_{(\mathrm{w}+2)} < \tfrac{Q}{\gamma_0}\right] \\ &= F_\Psi\left(\sqrt{\tfrac{\alpha_1}{\gamma_0}}\right) \times F_{g_{(\mathrm{w}+2)}}\left(\tfrac{Q}{\gamma_0}\right) \end{aligned} \tag{12}$$

where the estimated channel gain $g_{(w+2)} = \left|h_{(w+2)}\right|^2$ is exponentially distributed RVs with CDF $F_{g_{(\mathrm{w}+2)}}(x) = 1 - e^{-\lambda_{(\mathrm{w}+2)}x}$ and PDF $f_{g_{(\mathrm{w}+2)}}(x) = \lambda_{(\mathrm{w}+2)}e^{-\lambda_{(\mathrm{w}+2)}x}$ [22].

And substituting (11) into (12), we obtain

$$\Upsilon_1 = \frac{\gamma\left(a+1, \frac{1}{b}\sqrt{\frac{\alpha_1}{\gamma_0}}\right)}{\Gamma(a+1)} \times \left(1 - e^{-\lambda_{(\mathrm{w}+2)}Q/\gamma_0}\right) \tag{13}$$

Next, the Υ_2 in the (9) is determined as followed

$$\begin{aligned} \Upsilon_2 &= \Pr\left[\Psi < \underbrace{\sqrt{\alpha_1/Q}}_{\alpha_2}\sqrt{g_{(\mathrm{w}+2)}}, g_{(\mathrm{w}+2)} \geq \underbrace{Q/\gamma_0}_{\alpha_3}\right] \\ &= \int_{\alpha_3}^{\infty} f_{g_{(\mathrm{w}+2)}}(x) \times F_\Psi(\alpha_2\sqrt{x})\, dx \end{aligned} \tag{14}$$

Substituting (11) into (14), we obtain

$$\Upsilon_2 = \int_{\alpha_3}^{\infty} \frac{\lambda_{(\mathrm{w}+2)}}{\Gamma(a+1)}e^{-\lambda_{(\mathrm{w}+2)}x}\gamma\left(a+1, \frac{\alpha_2}{b}\sqrt{x}\right) dx \tag{15}$$

After some analysis we have the following result of the Υ_2 in two forms: the integral expression and the infinite sum expression with the formulas (16) and (17), respectively.

$$\begin{aligned}\Upsilon_2 = {} & 2^{-\left(a+\frac{1}{2}\right)}\left(\tfrac{\alpha_2}{b}\right)^{\left(a+\frac{1}{2}\right)}{\lambda_{(\mathrm{w}+2)}}^{-\frac{1}{2}(a+1/2)}\times \\ & \times W_{-\frac{1}{2}(a+1/2),-\frac{1}{4},\left(\frac{{\alpha_2}^2}{4b^2\lambda_{(\mathrm{w}+2)}}\right)}+ \\ & + \int_0^{\alpha_3} \tfrac{\lambda_{(\mathrm{w}+2)}}{\Gamma(a+1)} e^{-\lambda_{(\mathrm{w}+2)}x}\gamma\left(a+1,\tfrac{\alpha_2}{b}\sqrt{x}\right)dx\end{aligned} \tag{16}$$

$$\begin{aligned}\Upsilon_2 = {} & 2^{-\left(a+\frac{1}{2}\right)}\left(\tfrac{\alpha_2}{b}\right)^{\left(a+\frac{1}{2}\right)}{\lambda_{(\mathrm{w}+2)}}^{-\frac{1}{2}(a+1/2)}\times \\ & \times W_{-\frac{1}{2}(a+1/2),-\frac{1}{4},\left(\frac{{\alpha_2}^2}{4b^2\lambda_{(\mathrm{w}+2)}}\right)}+ \\ & + \tfrac{\lambda_{(\mathrm{w}+2)}}{\Gamma(a+1)}\sum_{n=0}^{\infty}\tfrac{(-1)^n}{n!(a+1+n)}\left(\lambda_{(\mathrm{w}+2)}\right)^{-\left(\frac{1}{2}(a+1+n)+1\right)}\times \\ & \times\gamma\left(\tfrac{1}{2}(a+1+n)+1,\lambda_{(\mathrm{w}+2)}\alpha_3\right)\end{aligned} \tag{17}$$

Substituting (13) and (16) or (17) into (9), we obtain $OP_{S_p}^{out}$ in (18) or (19) at the top of next page.

Corollary 1: In special case as $\gamma_0 \to +\infty$ then $e^{-\lambda_{(\mathrm{w}+2)}Q/\gamma_0} \to 1 \Rightarrow \Upsilon_1 \to 0$ and $\alpha_3 \to +\infty$ we obtain asymptotic expression as

$$\begin{aligned}OP_{S_p}^{out,\gamma_0\to\infty} = {} & 2^{-\left(a+\frac{1}{2}\right)}\left(\tfrac{\alpha_2}{b}\right)^{\left(a+\frac{1}{2}\right)}{\lambda_{(\mathrm{w}+2)}}^{-\frac{1}{2}(a+1/2)}\times \\ & \times W_{-\frac{1}{2}(a+1/2),-\frac{1}{4},\left(\frac{{\alpha_2}^2}{4b^2\lambda_{(\mathrm{w}+2)}}\right)}\end{aligned} \tag{20}$$

Corollary 2: In special case as $Q \to +\infty$ then $e^{-\lambda_{(\mathrm{w}+2)}Q/\gamma_0} \to 0$, $\alpha_2 \to 0$ and $\alpha_3 \to +\infty$ we obtain asymptotic expression as

$$OP_{S_p}^{out,Q\to\infty} = \frac{\gamma\left(a+1,\frac{1}{b}\sqrt{\frac{\alpha_1}{\gamma_0}}\right)}{\Gamma(a+1)} \tag{21}$$

IV. Results and discussions

This section presents analysis and simulation results in terms of outage probabilities of the proposed RIS-UTW scheme. The simulation results are performed by the Monte Carlo method to validate the analyzed expressions. Coordinates of the nodes S_1, S_2, the PR and the RIS are set as $\mathrm{S}_1\,(0,0)$, $\mathrm{S}_2\,(1,0)$, $\mathrm{PR}\,(x_{\mathrm{PR}},y_{\mathrm{PR}})$, $\mathrm{RIS}\,(x_{\mathrm{R}},y_{\mathrm{R}})$, where $0 < x_{\mathrm{R}} < 1$. The normalized distances are calculated from the coordinates as $d_1 = \sqrt{x_{\mathrm{R}}^2 + y_{\mathrm{R}}^2}$, $d_2 = \sqrt{(1-x_{\mathrm{R}})^2 + y_{\mathrm{R}}^2}$, $d_3 = \sqrt{(x_{\mathrm{PR}})^2 + (y_{\mathrm{PR}})^2}$, and $d_4 = \sqrt{(1-x_{\mathrm{PR}})^2 + y_{\mathrm{PR}}^2}$. It is assumed that the threshold data rate and the path-loss exponent are fixed by $R_{\mathrm{th}} = 1(bits/s/Hz)$ and $\beta = 3$, and Q (dB) on the x-axis is defined as $Q = 10 \times \log_{10}(I/N_o)$ (dB). Markers denote simulated results.

Figure 2 shows the exact and asymptotic outage probabilities of the secondary sources S_1 and S_2 versus Q (dB) as formula (18) and (19) when $\gamma_0 = -15(dB)$, $T \in \{2,5,8\}$, $x_{\mathrm{R}} = 0.5$, $y_{\mathrm{R}} = -0.5$, $x_{\mathrm{PR}} = 0.5$, $y_{\mathrm{PR}} = 1$. Firstly, as selecting the above parameters, we have a symmetrical model with normalized distances $d_1 = d_2$, and $d_3 = d_4$, so the lines drawing the two sources outage probabilities nearly overlap. Secondly, the outage probabilities of both sources decrease as the interference constraint parameters Q increases in the region Q value is small and attains a saturation (floor) value in the high Q ones. Due to large values of Q, the transmit powers of the nodes S_1, S_2 increase as in (1) which correspond to large SNRs to decode the data x_1, x_2 in (4) and (8). And the transmit powers in (1) also have a limit by the maximum power of each source so the transmit powers will attain a saturation when Q achieves a high threshold value. Moreover, when the number of metasurfaces increases, the system outage probability decreases, or in other words, the system performance increases proportionally with the number of metasurfaces. Besides, in Fig 2, the outage probabilities of the secondary sources are plotted according to two analytical formulas in the infinite sum form (18) and the integral form (19). The results show that the curves represented by the integral formula coincides with the Monte Carlo simulation lines, while the curves represented by the infinite sum (with the first 25 terms selected) is closer to the simulation curves in case of the number of the RIS reflective cell increased.

Figure 3 considers the outage probabilities of the secondary sources S_1 and S_2 versus $Pmax/N_0$(dB) when $Q = -10$ (dB), $T \in \{2,5,8\}$, $x_{\mathrm{R}} = 0.5$, $y_{\mathrm{R}} = -0.5$, $x_{\mathrm{PR}} = 0.5$, $y_{\mathrm{PR}} = 1$. Firstly, similar to Fig. 2 with these selected parameters, Fig.3 also has the outage probabilities of the two sources overlap. Next, the outage probabilities of the sources quickly decrease as $Pmax/N_0$ (dB) increases to about -10 dB, then they remain constant even though $Pmax/N_0$(dB) still increases. It shows that the higher the maximum capacity the hardware is able to handle, the better the system performance is, however it has a saturation value because the transmit power depends on two parameters like formula (1). Furthermore, the system performance increases proportionally with the number of metasurfaces as Fig. 2.

Fig. 4 examines the effect of the distances between PR and secondary sources on the outage probability of the secondary system versus Q. When this distances increase leading to the outage probabilities of the system decrease. We have the result because in (4) and (8) the SINRs decrease when the transmit power of the secondary sources increases. And the transmit power of the secondary sources increases when the distances between PR and secondary increase due to the interference effect of the secondary network to PR decreases as in formula (1). Finally, the asymptotic and exact theory analysis lines of the outage probabilities match well with their Monte Carlo simulation ones.

V. Conclusions

In this paper, we proposed and analyzed the underlay two-way RIS scheme with two secondary sources and a primary receiver, known as the UTW-RIS. To evaluate the system performance, the paper investigated the outage probability via parameters such as Q (dB), $Pmax/N_0$(dB), number of reflected elements of RIS. The notable results are that the system outage probabilities decrease a lot when the number of

$$OP_{S_p}^{out} = \frac{\gamma\left(a+1, \frac{1}{b}\sqrt{\frac{\alpha_1}{\gamma_0}}\right)}{\Gamma(a+1)} \times \left(1 - e^{-\lambda_{(\mathrm{w}+2)}Q/\gamma_0}\right) + 2^{-\left(a+\frac{1}{2}\right)}\left(\frac{\alpha_2}{b}\right)^{\left(a+\frac{1}{2}\right)}{\lambda_{(\mathrm{w}+2)}}^{-\frac{1}{2}(a+1/2)} \times \\ \times W_{-\frac{1}{2}(a+1/2),-\frac{1}{4},\left(\frac{{\alpha_2}^2}{4b^2\lambda_{(\mathrm{w}+2)}}\right)} + \int_0^{\alpha_3} \frac{\lambda_{(\mathrm{w}+2)}}{\Gamma(a+1)} e^{-\lambda_{(\mathrm{w}+2)}x} \gamma\left(a+1, \frac{\alpha_2}{b}\sqrt{x}\right) dx \tag{18}$$

$$OP_{S_p}^{out} = \frac{\gamma\left(a+1, \frac{1}{b}\sqrt{\frac{\alpha_1}{\gamma_0}}\right)}{\Gamma(a+1)} \times \left(1 - e^{-\lambda_{(\mathrm{w}+2)}Q/\gamma_0}\right) + 2^{-\left(a+\frac{1}{2}\right)}\left(\frac{\alpha_2}{b}\right)^{\left(a+\frac{1}{2}\right)}{\lambda_{(\mathrm{w}+2)}}^{-\frac{1}{2}(a+1/2)} \times W_{-\frac{1}{2}(a+1/2),-\frac{1}{4},\left(\frac{{\alpha_2}^2}{4b^2\lambda_{(\mathrm{w}+2)}}\right)} + \\ + \frac{\lambda_{(\mathrm{w}+2)}}{\Gamma(a+1)} \sum_{n=0}^{\infty} \frac{(-1)^n}{n!(a+1+n)} \left(\lambda_{(\mathrm{w}+2)}\right)^{-\left(\frac{1}{2}(a+1+n)+1\right)} \times \gamma\left(\frac{1}{2}(a+1+n)+1, \lambda_{(\mathrm{w}+2)}\alpha_3\right) \tag{19}$$

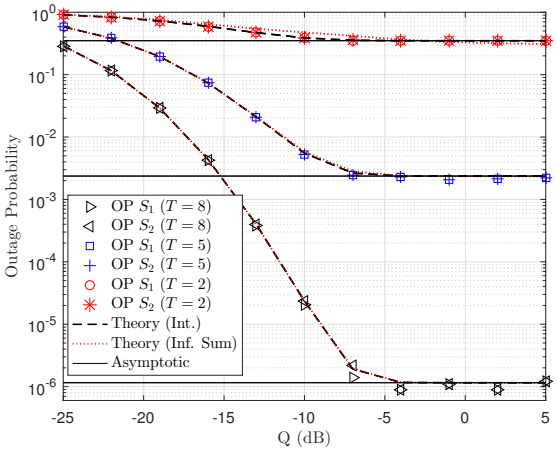

Fig. 2. The outage probabilities of the secondary sources S_1 and S_2 versus Q (dB) when $\gamma_0(dB) = -15(dB)$, $T \in \{2, 5, 8\}$, $x_{\mathrm{R}} = 0.5$, $y_{\mathrm{R}} = -0.5$, $x_{\mathrm{PR}} = 0.5$, $y_{\mathrm{PR}} = 1$.

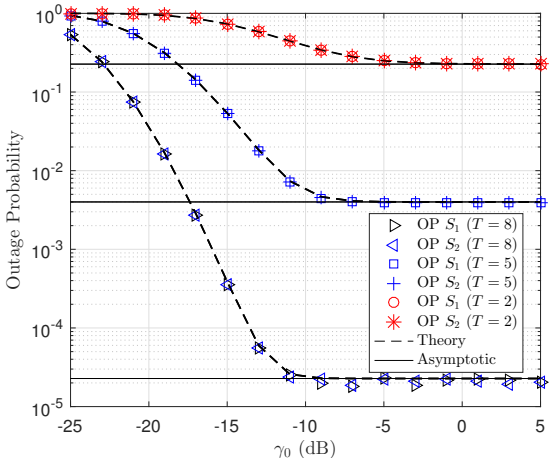

Fig. 3. The outage probabilities of the secondary sources S_1 and S_2 versus $\gamma_0 = Pmax/N_0$(dB) when $Q = -10$ (dB), $T \in \{2, 5, 8\}$, $x_{\mathrm{R}} = 0.5$, $y_{\mathrm{R}} = -0.5$, $x_{\mathrm{PR}} = 0.5$, $y_{\mathrm{PR}} = 1$.

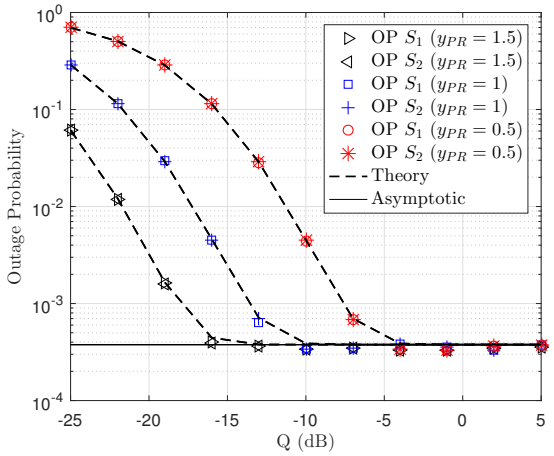

Fig. 4. The outage probabilities of the secondary sources S_1 and S_2 versus Q (dB) when $\gamma_0(dB) = -15(dB)$, $T = 8$, $x_{\mathrm{R}} = 0.5$, $y_{\mathrm{R}} = -0.5$, $x_{\mathrm{PR}} = 0.5$, $y_{\mathrm{PR}} \in \{0.5, 1, 1.5\}$.

reflected elements increase. Besides, the system outage probabilities decrease fastly when Q or $Pmax/N_0(dB)$ increase at their small value region, and reach the saturation value at their high value region. Finally, the analysis results of the outage probabilities were validated by the Monte Carlo simulations.

REFERENCES

[1] E. Basar, M. Di Renzo, J. De Rosny, M. Debbah, M.-S. Alouini, and R. Zhang, "Wireless communications through reconfigurable intelligent surfaces," IEEE Access, vol. 7, pp. 116753-116773, 2019.

[2] C. Liaskos, S. Nie, A. Tsioliaridou, A. Pitsillides, S. Ioannidis, and I. Akyildiz, "A new wireless communication paradigm through software-controlled metasurfaces," IEEE Communications Magazine, vol. 56, pp. 162-169, 2018.

[3] A.-A. A. Boulogeorgos and A. Alexiou, "Performance Analysis of Reconfigurable Intelligent Surface-Assisted Wireless Systems and Comparison With Relaying," IEEE Access, vol. 8, pp. 94463-94483, 2020.

[4] B. Zheng, M. Wen, C.-X. Wang, X. Wang, F. Chen, J. Tang, et al., "Secure NOMA based two-way relay networks using artificial noise and full duplex," IEEE Journal on Selected Areas in Communications, vol. 36, pp. 1426-1440, 2018.

[5] H. Cui, M. Ma, L. Song, and B. Jiao, "Relay selection for two-way full duplex relay networks with amplify-and-forward protocol," IEEE Transactions on Wireless Communications, vol. 13, pp. 3768-3777, 2014.

[6] T.-T. T. Dao, N.-L. Nguyen, H.-N. Nguyen, S.-P. Le, D.-T. Do, Q. Nguyen, et al., "Exploiting secure performance of full-duplex decode and forward in optimal relay selection networks," Elektronika IR Elektrotechnika, vol. 24, 2018.

[7] I. F. Akyildiz, W.-Y. Lee, M. C. Vuran, and S. Mohanty, "NeXt generation/dynamic spectrum access/cognitive radio wireless networks: A survey," Computer networks, vol. 50, pp. 2127-2159, 2006.

[8] A. Goldsmith, S. A. Jafar, I. Maric, and S. Srinivasa, "Breaking spectrum gridlock with cognitive radios: An information theoretic perspective," Proceedings of the IEEE, vol. 97, pp. 894-914, 2009.

[9] Y. Chen, T. Zhang, Y. Liu, and X. Qiao, "Physical Layer Security in NOMA-Enabled Cognitive Radio Networks With Outdated Channel State Information," IEEE Access, vol. 8, pp. 159480-159492, 2020.

[10] Q. Li and L. Yang, "Beamforming for cooperative secure transmission in cognitive two-way relay networks," IEEE Transactions on Information Forensics and Security, vol. 15, pp. 130-143, 2019.

[11] R. T. Al-Zubi, M. T. Abu Issa, O. Jebreil, K. A. Darabkh, and Y. Khattabi, "Outage performance of cognitive two-way amplify-and-forward relay network under different transmission schemes," Transactions on Emerging Telecommunications Technologies, p. e4004, 2020.

[12] P. N. Son, T. T. Duy, and K. Ho-Van, "SIC-Coding Schemes for Underlay Two-Way Relaying Cognitive Networks," Wireless Communications and Mobile Computing, vol. 2020, 2020.

[13] X. Zhang, Z. Zhang, J. Xing, R. Yu, P. Zhang, and W. Wang, "Exact outage analysis in cognitive two-way relay networks with opportunistic relay selection under primary user's interference," IEEE Transactions on Vehicular Technology, vol. 64, pp. 2502-2511, 2014.

[14] J. Yuan, Y.-C. Liang, J. Joung, G. Feng, and E. G. Larsson, "Intelligent reflecting surface (IRS)-enhanced cognitive radio system," in ICC 2020-2020 IEEE International Conference on Communications (ICC), 2020, pp. 1-6.

[15] D. Xu, X. Yu, Y. Sun, D. W. K. Ng, and R. Schober, "Resource allocation for IRS-assisted full-duplex cognitive radio systems," IEEE Transactions on Communications, vol. 68, pp. 7376-7394, 2020.

[16] D. Xu, X. Yu, and R. Schober, "Resource allocation for intelligent reflecting surface-assisted cognitive radio networks," in 2020 IEEE 21st International Workshop on Signal Processing Advances in Wireless Communications (SPAWC), 2020, pp. 1-5.

[17] S. Atapattu, R. Fan, P. Dharmawansa, G. Wang, and J. Evans, "Two–way communications via reconfigurable intelligent surface," in 2020 IEEE Wireless Communications and Networking Conference (WCNC), 2020, pp. 1-6.

[18] S. Atapattu, R. Fan, P. Dharmawansa, G. Wang, J. Evans, and T. A. Tsiftsis, "Reconfigurable intelligent surface assisted two–way communications: Performance analysis and optimization," IEEE Transactions on Communications, vol. 68, pp. 6552-6567, 2020.

[19] I. S. G. a. I. M. Ryzhik, Table of integrals, series, and products, Seventh ed.: Elsevier, 2007.

[20] H. Van Toan, V.-N. Q. Bao, and H. Nguyen-Le, "Cognitive two-way relay systems with multiple primary receivers: exact and asymptotic outage formulation," IET Communications, vol. 11, pp. 2490-2497, 2017.

[21] S. Primak, V. Kontorovich, and V. Lyandres, "Stochastic methods and their applications to communications," Stochastic Differential Equations Approach. John Wiley and Sons, 2004.

[22] P. N. Son and H. Y. Kong, "Exact outage probability of two-way decode-and-forward scheme with opportunistic relay selection under physical layer security," Wireless personal communications, vol. 77, pp. 2889-2917, 2014.